

## LIQUID CRYSTALS

## Hybrid molecular-colloidal liquid crystals

Haridas Mundoor,<sup>1</sup> Sungoh Park,<sup>1</sup> Bohdan Senyuk,<sup>1</sup>  
Henricus H. Wensink,<sup>2</sup> Ivan I. Smalyukh<sup>1,3,4\*</sup>

Order and fluidity often coexist, with examples ranging from biological membranes to liquid crystals, but the symmetry of these soft-matter systems is typically higher than that of the constituent building blocks. We dispersed micrometer-long inorganic colloidal rods in a nematic liquid crystalline fluid of molecular rods. Both types of uniaxial building blocks, while freely diffusing, interact to form an orthorhombic nematic fluid, in which like-sized rods are roughly parallel to each other and the molecular ordering direction is orthogonal to that of colloidal rods. A coarse-grained model explains the experimental temperature-concentration phase diagram with one biaxial and two uniaxial nematic phases, as well as the orientational distributions of rods. Displaying properties of biaxial optical crystals, these hybrid molecular-colloidal fluids can be switched by electric and magnetic fields.

A vast variety of anisotropic building blocks, such as organic molecules, filamentous viruses, and graphene flakes, self-organize to form nematic liquid crystals (NLCs) (*1*). NLCs can flow because of the lack of correlation in positions of their freely diffusing building blocks, such as rodlike molecules (*1*). However, the long-range average orientational order of such rods along a direction dubbed “director” yields anisotropic properties typically associated with crystalline solids (*1*). These nonpolar uniaxial NLCs exhibit the  $D_{\infty h}$  point group symmetry, but fluidity and order could also coexist in fundamentally different ways (*1*). The most sought-after structures are orthorhombic, optically biaxial NLCs, which were envisaged as nematic fluids of brick-shaped building blocks (*2*), with long-range orientational order of both long and short axes of the bricks along the mutually orthogonal directors. Most strategies to realize such NLCs in micellar (*3*), small-molecule (*4*), polymeric (*5*), colloidal (*6*), and other systems (*7*) relied on the designs of bricklike and other biaxial building blocks. We show that such biaxial NLCs can be formed by rodlike building blocks in a hybrid molecular-colloidal soft-matter system.

Small-molecule NLCs are often used as host media to form colloidal dispersions (*8*). However, colloidal particles are typically spheres or weakly shape-anisotropic rods and discs treated to induce strong boundary conditions to harness the elastic interactions for self-assembly

with well-defined relative positions and orientations of anisotropic inclusions coupled to the nematic director (*9–11*). We used bare, charged inorganic colloidal nanorods with high aspect ratios; these nanorods spontaneously form their own nematic states when dispersed in both isotropic and nematic phases of the NLC host. The average direction of ordering of nanorods is orthogonal to that of the small molecules in the nematic phase (Fig. 1). Analytical modeling of interactions between colloidal rods and the anisotropic molecular interactions at their surfaces explains the temperature-concentration phase diagram and experimental orientational distributions in the hybrid molecular-colloidal NLC. Within the orthorhombic phase, owing to anisotropic interactions, the molecular host induces a biaxial orientational distribution of the nanorods, which, in turn, induce biaxiality in the molecular host.

Hydrothermally synthesized (*12*) nanorods were pre-engineered for luminescence-based imaging of their orientations (*13*). The rods were treated with hydrochloric acid to achieve a length-to-diameter aspect ratio between 40 and 110 via slow etching (Fig. 1, B and C, and fig. S1) and then dispersed in a pentylcyanobiphenyl (5CB) NLC (*13*). These dispersions were infiltrated into glass cells (about 2.5 cm by 2.5 cm) with 10- to 60- $\mu\text{m}$  gap thickness or rectangular capillaries (0.2 mm by 2.0 mm). Monodomain NLC samples were obtained by treating the inner surfaces of cells and capillaries for perpendicular or tangential boundary conditions for the director  $\mathbf{n}_m$  describing the average orientation of molecules. Gravity and electrophoresis were used to concentrate nanorods (*13*). Within dispersions, surfaces of bare nanorods spontaneously induced weak perpendicular boundary conditions for  $\mathbf{n}_m$ . Surface charging of individual nanorods was controlled within  $Z^*e \approx +(50 \text{ to } 250)e$  (where  $e$  is the elementary charge and  $Z^*$  is the number of effective elementary charges on a nanorod's

surface) and characterized by probing the electrophoretic mobility of the rods. Debye screening length ( $\xi_D$ ) in the nonpolar 5CB NLC was varied from 0.1 to 2.1  $\mu\text{m}$ . Phase diagrams for  $\xi_D \approx 120 \text{ nm}$  and  $Z^*e \approx +250e$  (*13*) showed no dependence on capillary or cell dimensions.

Nanorods tend to orient orthogonally to  $\mathbf{n}_m$  (Fig. 1). They induce weak elastic distortions of molecular alignment, in contrast to microparticles (*11, 14*), which induce bulk defects, but similar to other nanoparticles with soft perpendicular surface boundary conditions (*15, 16*) (Fig. 1D and fig. S2). To minimize the overall free energy, elastic distortions compete with the cost of deviations of  $\mathbf{n}_m$  away from the local perpendicular boundary conditions at the particles' surfaces (Fig. 1D) (*13*). The biaxial molecular-colloidal NLC (Fig. 1, A to E) arises from the host-mediated electrostatic and elastic interactions between nanorods at modestly high colloidal volume fractions  $\phi_c$ , which spontaneously select the direction of colloidal ordering  $\mathbf{n}_c$  from a manifold of orientations defined by a plane orthogonal to  $\mathbf{n}_m$ . In a cell with  $\mathbf{n}_m$  orthogonal to substrates (Fig. 1, E to G),  $\mathbf{n}_c$  spontaneously aligns parallel to substrates and its orientation can be controlled by electric and magnetic fields. In a cell with in-plane  $\mathbf{n}_m$ ,  $\mathbf{n}_c$  spontaneously aligns orthogonally to substrates (Fig. 1H) but can be switched to the in-plane orientation orthogonal to  $\mathbf{n}_m$  by a 50- to 100-mT magnetic field normal to the substrates (Fig. 1I) (*13*). Rotation of samples placed between crossed polarizers around  $\mathbf{n}_m$  yields minima of transmitted intensity when  $\mathbf{n}_c$  is either parallel or perpendicular to crossed polarizers (Fig. 1F) and a maximum when  $\mathbf{n}_c$  is at  $45^\circ$  (Fig. 1G). Rotation around  $\mathbf{n}_c$  yields minima of transmitted intensity when  $\mathbf{n}_m$  is parallel or perpendicular to polarizers (Fig. 1J) and a maximum when  $\mathbf{n}_m$  is at  $45^\circ$  (Fig. 1K). Luminescence imaging (Fig. 1, E, H, and I, and movies S1 and S2) reveals that nanorods freely diffuse while exhibiting orientational order but no positional order (Fig. 1A).

The biaxial  $D_{2h}$  orthorhombic symmetry of our molecular-colloidal NLC is characterized by a triplet of directors:  $\mathbf{n}_m$ ,  $\mathbf{n}_c$  and  $\mathbf{n}_l$  orthogonal to both  $\mathbf{n}_m$  and  $\mathbf{n}_c$  (Fig. 2). Nanorods are uniaxial solid nanocrystals with an optical axis along their long axis and extraordinary and ordinary refractive indices  $N_{ec} = 1.46$  and  $N_{oc} = 1.49$  (*17*). In the absence of colloidal inclusions, the molecular host is also a uniaxial crystal with indices  $N_{em} = 1.74$  and  $N_{om} = 1.54$  (*18*). However, the molecular-colloidal composite NLC is a biaxial optical crystal with three principal refractive indices and an optical indicatrix (Fig. 2B). These emergent properties arise both from the orthogonal alignment of  $\mathbf{n}_m$  and  $\mathbf{n}_c$  and also from the low symmetry of orientational distributions of molecular and colloidal rods due to anisotropic interactions between them (e.g., colloidal rods locally perturb orientations of molecular rods, as shown in Figs. 1D and 2A). Using a Berek compensator inserted between crossed polarizers after the NLC in the geometries depicted in Fig. 1, G and K, we measured the two characteristic optical anisotropies of the biaxial NLC at different  $\phi_c$ :

<sup>1</sup>Department of Physics and Soft Materials Research Center, University of Colorado, Boulder, CO 80309, USA. <sup>2</sup>Laboratoire de Physique des Solides, CNRS, Université Paris-Sud, Université Paris-Saclay, 91405 Orsay, France. <sup>3</sup>Department of Electrical, Computer, and Energy Engineering, Materials Science and Engineering Program, University of Colorado, Boulder, CO 80309, USA. <sup>4</sup>Renewable and Sustainable Energy Institute, National Renewable Energy Laboratory and University of Colorado, Boulder, CO 80309, USA.

\*Corresponding author. Email: ivan.smalyukh@colorado.edu

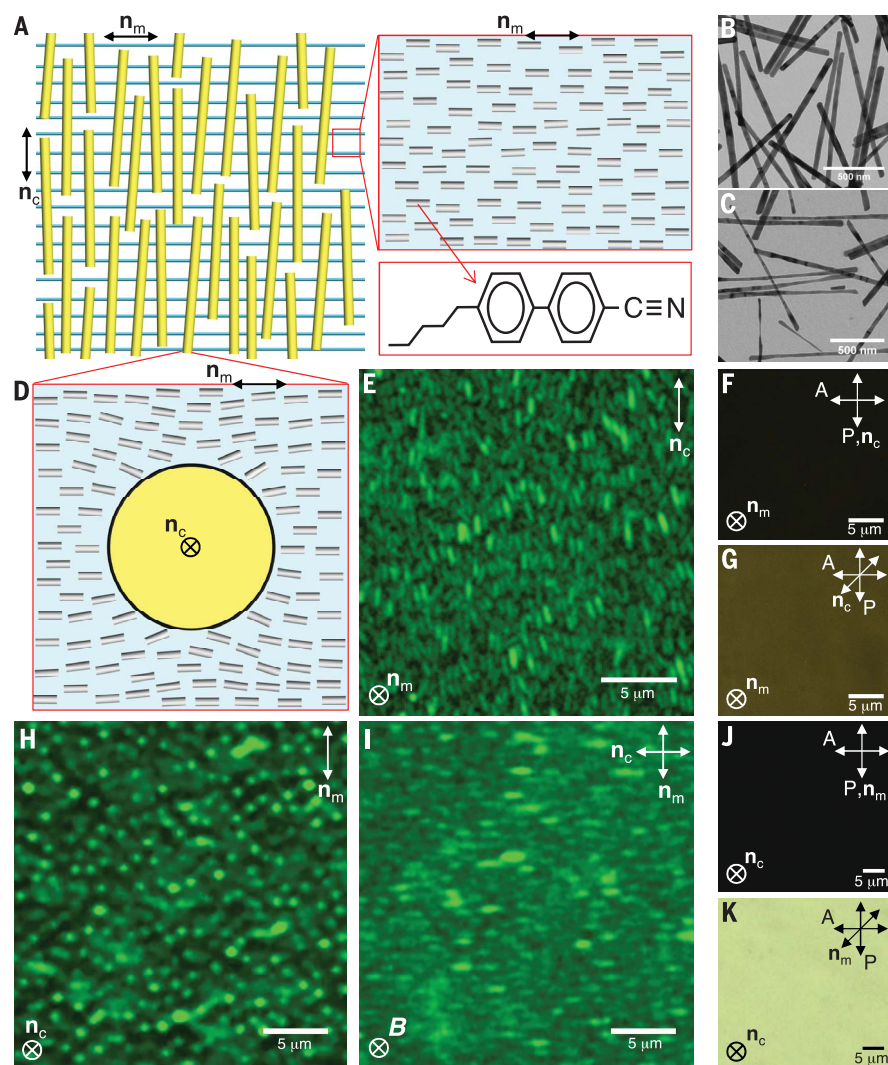


**Fig. 1. Structure and characterization of an orthorhombic biaxial NLC.** (A) Schematic representation of the hybrid molecular-colloidal NLC, with the insets showing (top right) molecular ordering and (bottom right) chemical structure of a 5CB molecule. (B and C) Transmission electron micrographs of nanorods (B) before and (C) after acid treatment. (D) Schematic representation of distortions of the molecular alignment around a nanorod with soft perpendicular boundary conditions. (E) Upconversion-based luminescence confocal microscopy image of the nanorods, showing their alignment along  $n_c$ , orthogonal to  $n_m$ . (F and G) Polarizing optical micrographs of a biaxial NLC between crossed polarizer P and analyzer A when  $n_c$  is at (F)  $0^\circ$  and (G)  $45^\circ$  with respect to P. (H and I) Confocal luminescence images of nanorods in a biaxial NLC when the particles are (H) aligned perpendicular to  $n_m$  and then (I) switched with a magnetic field  $B$  applied perpendicular to  $n_m$  and substrates. (J and K) Polarizing optical micrograph of a biaxial NLC viewed between crossed polarizers when  $n_m$  is at (J)  $0^\circ$  and (K)  $45^\circ$  with respect to P.

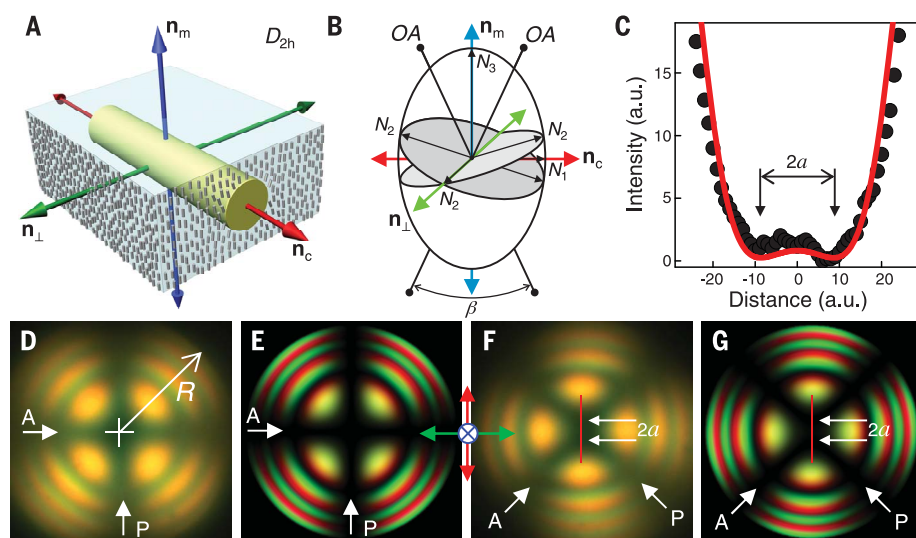


**Fig. 2. Optical properties and conoscopic images of a biaxial NLC.** (A) Schematic representation of a coarse-grained building block of the NLC formed by a nanorod in a molecular nematic host. Three double arrows (red, green, and blue) depict the triplet of directors. (B) Optical indicatrix of a biaxial NLC with orthorhombic symmetry. The optical axes, at an angle  $\beta$  to each other, are designated "OA" and confined to the plane formed by  $n_c$  and  $n_m$ . (C) Experimental (black circles) and computer-simulated (red line) intensity profiles along the red lines in the conoscopic images shown in (F) and (G), respectively. a.u., arbitrary units. (D to G) Conoscopic images obtained experimentally [(D) and (F)] and via computer simulations [(E) and (G)] for the orientations of the plane containing the two optical axes parallel to the polarizer P [(D) and (E)] and at  $45^\circ$  to it [(F) and (G)], as marked on the images. A, analyzer. The ratio  $a/R \approx 0.059$  (where  $2a$  is the closest distance between split isogyres and  $R$  is the radius of the conoscopic image) obtained from the images is consistent with refractive index measurements (13).

$\Delta N_{21} = N_2 - N_1 = (0.4 \text{ to } 1.1) \times 10^{-3}$  and  $\Delta N_{31} = N_3 - N_1 \approx 0.2$ . Values of  $\Delta N_{31} \gg \Delta N_{21}$  are common for biaxial optical crystals in both solid-state (19) and soft-matter (7, 20) systems, where typical biaxial birefringence is  $\sim 10^{-3}$ . Experimental conoscopic images, produced by optical

interference of diverging light rays traveling through a biaxial NLC (19), match the ones simulated with the use of separately measured  $\Delta N_{21}$  and  $\Delta N_{31}$  (Fig. 2, D to G). For  $\mathbf{n}_m$  along the microscope's axis and the NLC's plane containing optical axes oriented at  $45^\circ$  to the crossed

polarizers, conoscopic patterns of birefringent colors display splitting of dark bands (isogyres) characteristic of biaxial crystals (Fig. 2, C, F, and G) (7, 19), producing an estimate of the angle  $\beta \approx 5.9^\circ$  between the optical axes.

In addition to the biaxial state, the temperature-concentration phase diagram exhibits isotropic and two uniaxial phases, as well as two-phase coexistence regions (Fig. 3). At low  $\phi_c$  and temperatures  $T$ , nanorods orient randomly in a plane orthogonal to  $\mathbf{n}_m$  while retaining  $D_{\text{oh}}$  point group symmetry of the dispersion (Fig. 3, A to C), but there is a phase transition to the biaxial phase at  $\phi_c = \phi_{c\text{UB}} \approx 0.15\%$  (where  $\phi_{c\text{UB}}$  is the volume fraction at the uniaxial-to-biaxial transition). The temperature of the order-disorder transition for molecular rods of the nematic host ( $T^*$ ) decreases only slightly with increasing  $\phi_c$  up to 0.3% as compared with  $T^* \approx 35.3^\circ\text{C}$  of pristine 5CB (Fig. 3C). At  $T > T^*$ , the dispersion exhibits a transition from isotropic to uniaxial nematic phase at  $\phi_c = \phi_{c\text{IN}} \approx 0.26\%$  (where  $\phi_{c\text{IN}}$  is the volume fraction at the isotropic-to-nematic transition) (Fig. 3, C and D), as predicted by the Onsager's theory (21) with the electrostatic effects taken into account (13, 22). Two-phase coexistence regions appear at the high- $T$  isotropic-uniaxial and low- $T$  uniaxial-biaxial transitions (Fig. 3C). Luminescence imaging of nanorods reveals their orientations in different phases and geometries (Fig. 3 and fig. S2) and that  $\mathbf{n}_c$  spontaneously aligns normally to the confining plates in the high- $T$  uniaxial phase (Fig. 3D and movie S3) but is always orthogonal to  $\mathbf{n}_m$  within the low- $T$  biaxial phase, even when this forces  $\mathbf{n}_c$  to be parallel to substrates (Fig. 3E).

We separately characterize orientational distribution functions  $f_{c,m}$  that quantify probabilities of different orientations of colloids and molecules (denoted by "c" and "m") (Fig. 4). From the experimental  $f_{c,m}$ , we extract order parameters  $S_{c,m}$  and  $\Delta_{c,m}$  associated with colloidal and molecular rods to quantify their degree of ordering and biaxiality, respectively

$$S_{c,m} = \int_0^{2\pi} d\varphi \int_{-1}^1 d(\cos\theta) f_{c,m}(\theta, \varphi) P_2(\cos\theta) \quad (1)$$

$$\Delta_{c,m} = \int_0^{2\pi} d\varphi \int_{-1}^1 d(\cos\theta) f_{c,m}(\theta, \varphi) D(\theta, \varphi) \quad (2)$$

where  $\theta$  and  $\varphi$  are polar and azimuthal angles, respectively, describing molecular or colloidal orientations defined with respect to  $\mathbf{n}_m$ ;  $P_2(\cos\theta) = \frac{1}{2}(3\cos^2\theta - 1)$ ; and  $D(\theta, \varphi) = \sin^2\theta\cos 2\varphi$ . Using polarized Raman spectroscopy (fig. S3), we find that  $S_m$  in the biaxial phase is slightly lower than  $S_m$  of pristine 5CB (Fig. 4A). Moreover, the nanorod-induced biaxiality  $\Delta_m = 0.01$  to  $0.04$  shows a trend of increasing with  $T$ , opposite to that of  $S_m$ , though both parameters abruptly drop to zero at  $T^*$  (Fig. 4A). These findings are consistent with polarized three-photon-absorption-based fluorescence from the biphenyl groups of molecules characterized for both pure 5CB and the biaxial phase of the hybrid NLC (fig. S4). Direct luminescence imaging of nanorods

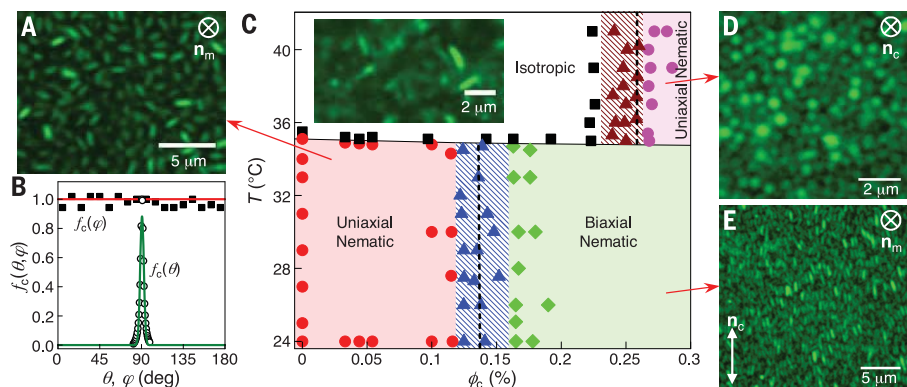


**Fig. 3. Phase diagram of a hybrid molecular-colloidal NLC.** (A) Confocal luminescence image of nanorods in 5CB at  $\phi_c \approx 0.054\%$  at room temperature. (B)  $f_c(\theta, \varphi)$  versus  $\theta$  and  $\varphi$  at  $\phi_c \approx 0.025\%$ , obtained by normalizing the maximum values of functions that fit experimental distributions. (C) Phase diagram of the hybrid molecular-colloidal system exhibiting uniaxial nematic, isotropic, biaxial nematic, and colloidal uniaxial phases. The inset is a confocal luminescence image of nanorods in a disordered state at  $\phi_c \approx 0.1\%$  and  $T = 38^\circ\text{C}$ . Red arrows indicate confocal luminescence images corresponding to different parts of the diagram. Dashed vertical lines denote theoretical predictions for  $\phi_{c\text{UB}}$  and  $\phi_{c\text{IN}}$ . (D) Confocal luminescence image of the colloidal uniaxial nematic state formed by nanorods at  $\phi_c \approx 0.272\%$  and  $T = 40^\circ\text{C}$ . (E) Confocal luminescence image showing nanorods in the biaxial phase at  $\phi_c \approx 0.172\%$  at room temperature.

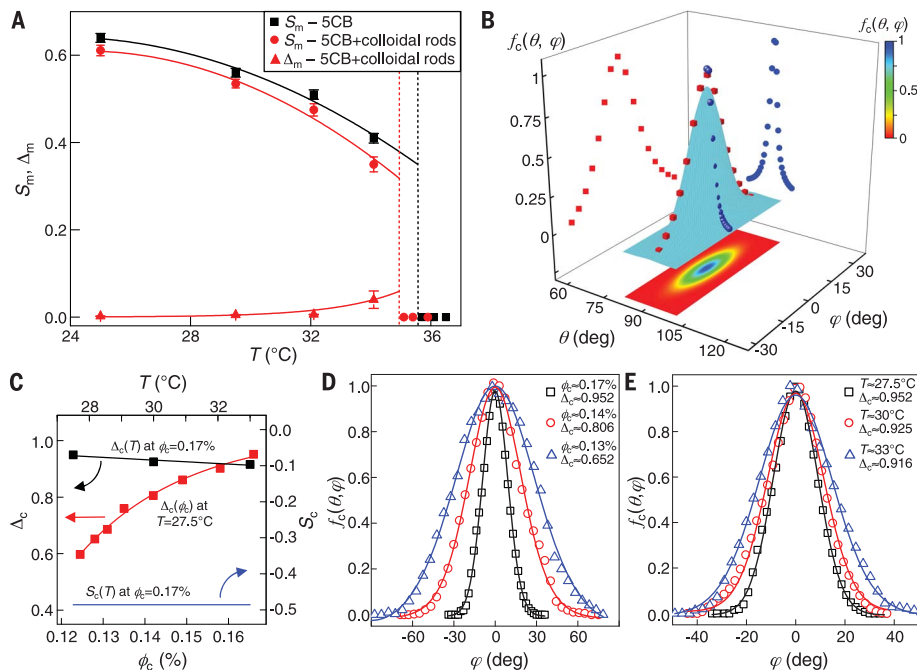


**Fig. 4. Order parameters and orientational distributions.** (A)  $S_m$  versus  $T$  for pure 5CB (black squares) and  $S_m$  (red circles) and  $\Delta_m$  (red triangles) for a biaxial phase at  $\phi_c = 0.17\%$  characterized by using Raman spectroscopy (13). (B)  $f_c(\theta, \varphi)$  versus angles  $\theta$  (blue symbols) and  $\varphi$  (red symbols) describing orientations of nanorods in a biaxial phase at  $\phi_c = 0.176\%$  and  $T = 27.5^\circ\text{C}$ . (C) Dependencies of  $\Delta_c$  (black squares) and  $S_c$  (blue curve) on temperature at  $\phi_c = 0.17\%$  and variation of  $\Delta_c$  (red squares) with  $\phi_c$  at room temperature. Arrows indicate the vertical axes corresponding to the curves. (D)  $f_c(\theta, \varphi)$  versus  $\varphi$  at room temperature and  $\phi_c = 0.17\%$  (black squares),  $0.14\%$  (red circles), and  $0.13\%$  (blue triangles). (E)  $f_c(\theta, \varphi)$  versus  $\varphi$  at  $\phi_c = 0.17\%$  and  $T = 27.5^\circ\text{C}$  (black squares),  $30^\circ\text{C}$  (red circles), and  $33^\circ\text{C}$  (blue triangles).

reveals their biaxial orientational distributions at different  $T$  and  $\phi_c$  (Fig. 4, B to E), as well as facile electric and magnetic switching of  $\mathbf{n}_c$  (fig. S5). In the vicinity of  $\phi_{cUB}$ , we detected only small changes of  $S_c \approx -0.49$  but find that  $\Delta_c$  jumps from zero to  $\approx 0.6$  at  $\phi_c \approx 0.12\%$  (in the beginning of the two-phase coexistence) and then increases with  $\phi_c$  to  $\approx 0.95$  at  $\phi_c > 0.16\%$  in the biaxial phase (Fig. 4C). Orientational distribution functions are biaxial for both molecular and colloidal rods, though biaxiality of colloidal ordering is much stronger than the weak induced biaxiality in molecular ordering (Fig. 4). The biaxial NLC is not merely a superposition of two uniaxial nematic molecular and colloidal states with orthogonal ordering directions. Anisotropic molecular interactions at interfaces of orientationally ordered nanorods lift the uniaxial symmetry of molecular order and, simultaneously, induce biaxiality in the distribution of colloidal nanorod orientations. Tensorial order parameters describing this behavior of molecules and colloids,  $\mathbf{Q}_{m,c} = \text{diag}\{S_{m,c}, (\Delta_{m,c} - S_{m,c})/2, -(\Delta_{m,c} + S_{m,c})/2\}$ , determine physical properties—such as the optical anisotropies characterized in Figs. 1 and 2—of the biaxial NLC.

Nematic order of pure 5CB emerges from anisotropic van der Waals interactions between molecules ( $I$ ), which are barely affected by the addition of nanorods, so that  $T^*$  decreases by only  $\sim 1^\circ\text{C}$  with increasing  $\phi_c < 0.3\%$  (Fig. 3C). The isotropic-nematic transition of charged nanorods with an effective aspect ratio  $l_{\text{eff}}$  upon increasing  $\phi_c$  at  $T > T^*$  due to electrostatic-modified steric interactions is also well understood (21, 22). Above  $\phi_{cIN} \approx 4/l_{\text{eff}}$ , consistent with the Onsager's theory, this order emerges upon maximizing the overall entropy of nanorods, which (despite lowering the number of states associated with rotational degrees of freedom) corresponds to an orientationally ordered state with low excluded volume and, thus, a large number of positional states accessible to nanorods. At  $T < T^*$  and  $\phi_c > \phi_{cUB}$ , nanorods align with long axes, on average, orthogonal to  $\mathbf{n}_m$  to minimize the free energy of the molecular nematic host (23, 24). The scalar order parameter  $S_c \approx -0.49$  (13), obtained from the experimental orientational distribution, is consistent with a model describing the anisotropic orientational distribution of nanorods in the presence of an aligning potential due to the nematic host (23, 24). By bringing individual nanorods within highly dilute dispersions near each other using laser tweezers, we find that they interact repulsively (fig. S6

and movie S4), showing no correlations in terms of their relative positions or orientations, which suggests that the colloidal ordering along  $\mathbf{n}_c$  at  $\phi_c > \phi_{cUB}$  emerges from Onsager-type collective behavior, though modified by direct interactions of nanorods with the nematic host and electrostatic repulsions. Because nanorod orientations in a molecular nematic host are effectively constrained to the plane orthogonal to  $\mathbf{n}_m$ , their degrees of freedom are reduced compared with those of isotropic hosts, so that ordering along  $\mathbf{n}_c$  emerges at  $\phi_{cUB} < \phi_{cIN}$  (Fig. 3C). For nanorods with soft boundary conditions, the orientational distribution function  $f_c$  derived using these assumptions reads (13)

$$f_c(\theta, \varphi) \propto \exp\left[\left(\frac{5}{4}\phi_c l_{\text{eff}} S_c - \sigma\right) P_2(\cos\theta)\right] \times \left[1 + \frac{15}{16}\phi_c l_{\text{eff}} \Delta_c D(\theta, \varphi)\right] \quad (3)$$

where  $\sigma$  is a dimensionless parameter describing the strength of nanorod interaction with the molecular nematic host. The order parameters  $S_c$  and  $\Delta_c$  are determined from fitting experimental data (Fig. 4B). This yields Onsager-type ordering along  $\mathbf{n}_c$  at  $\phi_{cUB} \approx 32[1 + 2/(3\sigma)]/(15l_{\text{eff}})$ . Since  $\sigma$  is large even in the limit of weak boundary conditions on nanorod surfaces,  $\phi_{cUB} \approx 32/(15l_{\text{eff}})$ , so that  $\phi_{cIN}/\phi_{cUB} \approx 1.9$ . Despite many assumptions and neglecting the anisotropy of dielectric constants within the NLC, which modifies electrostatic interactions, the prediction  $\phi_{cIN}/\phi_{cUB} \approx 1.9$  and the values of  $\phi_{cIN}$  and  $\phi_{cUB}$  agree with those experimentally determined for independently measured  $Z^*e$ ,  $\xi_D$ , and other parameters (Fig. 3C and figs. S7 to S9) (25, 26).

We have described a hybrid molecular-colloidal soft-matter system with orthorhombic biaxial orientational order and fluidity. Formed solely from uniaxial rodlike building blocks, this molecular-colloidal complex fluid features an unexpected self-organization into a biaxial NLC with the  $D_{2h}$  point group symmetry.

#### REFERENCES AND NOTES

1. P. M. Chaikin, T. C. Lubensky, *Principles of Condensed Matter Physics* (Cambridge Univ. Press, 1995).
2. M. J. Freiser, *Phys. Rev. Lett.* **24**, 1041–1043 (1970).
3. L. J. Yu, A. Saupé, *Phys. Rev. Lett.* **45**, 1000–1003 (1980).
4. B. R. Acharya, A. Primak, S. Kumar, *Phys. Rev. Lett.* **92**, 145506 (2004).
5. K. Severing, K. Saalwächter, *Phys. Rev. Lett.* **92**, 125501 (2004).

6. E. van den Pol, A. V. Petukhov, D. M. E. Thies-Weesie, D. V. Byelov, G. J. Vroege, *Phys. Rev. Lett.* **103**, 258301 (2009).
7. G. R. Luckhurst, T. J. Sluckin, Eds., *Biaxial Nematic Liquid Crystals: Theory, Simulation and Experiment* (Wiley, 2015).
8. P. Poulin, H. Stark, T. C. Lubensky, D. A. Weitz, *Science* **275**, 1770–1773 (1997).
9. H. Mundry, B. Senyuk, I. I. Smalyukh, *Science* **352**, 69–73 (2016).
10. Q. Liu, Y. Yuan, I. I. Smalyukh, *Nano Lett.* **14**, 4071–4077 (2014).
11. T. C. Lubensky, D. Pettey, N. Currier, H. Stark, *Phys. Rev. E* **57**, 610–625 (1998).
12. L. Wang, Y. Li, *Chem. Mater.* **19**, 727–734 (2007).
13. Materials and methods are available as supplementary materials.
14. B. Senyuk *et al.*, *Nature* **493**, 200–205 (2013).
15. R. W. Ruhwandl, E. M. Terentjev, *Phys. Rev. E* **56**, 5561–5565 (1997).
16. V. Tomar *et al.*, *Langmuir* **28**, 6124–6131 (2012).
17. D. Knowles, A. Cassanho, H. P. Jenssen, in *OSA Proceedings on Tunable Solid State Lasers*, M. L. Shand, H. P. Jenssen, Eds. [OSA Proceedings Series, Optical Society of America (OSA), 1989], vol. 5, pp. 139–145.
18. P. G. de Gennes, J. Prost, *The Physics of Liquid Crystals* (Clarendon Press, ed. 2, 1993).
19. E. E. Wahlstrom, *Optical Crystallography* (Wiley, ed. 4, 1969).
20. Y. Galerne *et al.*, *J. Chem. Phys.* **84**, 1732–1734 (1986).
21. L. Onsager, *Ann. N. Y. Acad. Sci.* **51**, 627–659 (1949).
22. G. J. Vroege, H. N. W. Lekkerkerker, *Rep. Prog. Phys.* **55**, 1241–1309 (1992).
23. Q. Liu *et al.*, *Phys. Rev. E* **89**, 052505 (2014).
24. Q. Liu *et al.*, *Phys. Rev. Lett.* **109**, 088301 (2012).
25. S. K. Sainis, J. W. Merrill, E. R. Dufresne, *Langmuir* **24**, 13334–13337 (2008).
26. A. Yethiraj, A. van Blaaderen, *Nature* **421**, 513–517 (2003).

#### ACKNOWLEDGMENTS

We thank P. Davidson, B. Fleury, Q. Liu, T. Lubensky, and L. Radzihovsky for discussions and technical assistance. **Funding:** This research was supported by the U.S. Department of Energy, Office of Basic Energy Sciences, Division of Materials Sciences and Engineering, under award ER46921, contract DE-SC0010305 with the University of Colorado at Boulder. **Author contributions:** H.M., S.P., B.S., and I.I.S. performed experiments and analyzed data. H.H.W. and I.I.S. developed theoretical models describing molecular-colloidal interactions and phase behavior. H.H.W. performed numerical calculations. I.I.S. conceived of the project, designed experiments, acquired funding, and wrote the manuscript, with the input from all authors. **Competing interests:** The authors declare no competing interests. **Data and materials availability:** All data are reported in the main text and supplementary materials.

#### SUPPLEMENTARY MATERIALS

www.sciencemag.org/content/360/6390/768/suppl/DC1  
Materials and Methods  
Figs. S1 to S9  
Additional Data  
References (27–34)  
Movies S1 to S4  
Data for Figure Plots

12 September 2017; accepted 13 April 2018  
10.1126/science.aap9359

## Hybrid molecular-colloidal liquid crystals

Haridas Mundoor, Sungoh Park, Bohdan Senyuk, Henricus H. Wensink and Ivan I. Smalyukh

*Science* **360** (6390), 768-771.  
DOI: 10.1126/science.aap9359

### Finding order in twos

In nematic liquid crystals, the local orientation of the molecules hovers around an average direction. The orientational control bestows unusual optical properties. In theory, with the right sort of two-dimensional shape, it should be possible to create nematics with biaxial ordering, but this has proven elusive. Mundoor *et al.* dispersed colloidal rods into a nematic solvent (see the Perspective by Poulin). Within a range of temperature and concentration, the rods ordered orthogonally to the solvent molecules, thus giving the mixture the type of properties that one would expect from a biaxial liquid crystal.

*Science*, this issue p. 768; see also p. 712

ARTICLE TOOLS	<a href="http://science.sciencemag.org/content/360/6390/768">http://science.sciencemag.org/content/360/6390/768</a>
SUPPLEMENTARY MATERIALS	<a href="http://science.sciencemag.org/content/suppl/2018/05/16/360.6390.768.DC1">http://science.sciencemag.org/content/suppl/2018/05/16/360.6390.768.DC1</a>
RELATED CONTENT	<a href="http://science.sciencemag.org/content/sci/360/6390/712.full">http://science.sciencemag.org/content/sci/360/6390/712.full</a>
REFERENCES	This article cites 27 articles, 3 of which you can access for free <a href="http://science.sciencemag.org/content/360/6390/768#BIBL">http://science.sciencemag.org/content/360/6390/768#BIBL</a>
PERMISSIONS	<a href="http://www.sciencemag.org/help/reprints-and-permissions">http://www.sciencemag.org/help/reprints-and-permissions</a>

Use of this article is subject to the [Terms of Service](#)

---

*Science* (print ISSN 0036-8075; online ISSN 1095-9203) is published by the American Association for the Advancement of Science, 1200 New York Avenue NW, Washington, DC 20005. The title *Science* is a registered trademark of AAAS.

Copyright © 2018 The Authors, some rights reserved; exclusive licensee American Association for the Advancement of Science. No claim to original U.S. Government Works